

Photoluminescence study of Au-Ag bimetallic nanoparticles supported on mesoporous silica SBA-15

Saba Estakhri¹, Elham Darabi*¹, Behrouz Akbari-Adergani², Seyed Mohammad Elahi¹

Abstract

Bimetallic Au-Ag nanoparticles with homogeneous dispersion in amine-modified SBA-15 mesoporous silica channels were successfully synthesized by the post-modification method. The obtained nanocomposites with different component ratios were studied by structural, Physico-chemical, and optical analysis. The structural and Physico-chemical properties were studied by X-ray diffraction (XRD), transmission electron microscopy (TEM), Fourier transform infrared (FTIR) spectroscopy, and nitrogen adsorption-desorption isotherm measurement (BET). The optical properties were characterized by photoluminescence (PL) and UV-Vis spectroscopy. The photoluminescence and absorption spectra were strongly affected by the change in the compositional ratio of gold to silver nanoparticles due to the interactions of Au-Ag nanoparticles, the configuration of conduction electrons, and their plasmonic properties. A significant enhancement was observed in the photoluminescence spectrum in the long-wavelength red emission at 640 nm for a one-to-one composition ratio of Au/Ag/SBA-15 nanocomposite. Since the light emission of most microorganisms is in the visible range, the nanocomposite produced can be proposed for applications in biosensor technology.

Keywords

Bimetallic Au/Ag nanoparticles; Mesoporous silica SBA-15; Photoluminescence; Plasmonic properties.

¹ Plasma Physics Research Center, Science and Research Branch, Islamic Azad University, Tehran, Iran

¹ Food and Drug Laboratories Research Center, Ministry of Health and Medical Education, Tehran, Iran

*Corresponding author: e.darabi@srbiau.ac.ir

1. Introduction

Mesoporous silicon nanostructures like SBA-15 have a unique place in the fields of materials design or materials science. Their exceptional properties such as large surface area, large pore volume, physical-chemical and thermal stability, permeability and biocompatibility are well known [1, 2]. The amazing property of mesoporous silica is its ability to support and encapsulate secondary materials such as nanoparticles. Metallic nanocomposites supported on SBA-15 are of great interest for optical applications, sensing and catalysis due to the high electron transfer rate and the plasmonic properties [1–6]. In recent years, bimetallic nanostructures; composed of two different metals have attracted much attention because the collective oscillation of conduction electrons in bimetallic nanostructures can differ from that of monometallic nanostructures, and their properties are significantly designed and modified by different choices of metals, composition, structure, size, and morphology can [7–10]. Among them, plasmonic noble metal nanoparticle alloys are very interesting due to the formation of new electronic structures, great plasmonic and catalytic activity, and their stability [10]. Since any compositional change modifies the properties, extensive studies on the fabrication and characterization of noble metal bimetallic nanos-

tructures for various applications have been reported [11–14]. When comparing different bimetallic nanostructures, gold and silver show a strong tendency to form alloys because they have almost identical lattice constants [14]. To increase efficacy and avoid nanoparticle agglomeration, bimetallic nanoparticles can be converted into nanocomposites. It was found that mesoporous silica SBA-15 carrying bimetallic nanoparticles was effective to enhance plasmonic and catalytic activity [15–17]. In this regard, attempts have been made to investigate the benefits of changes in surface, electronic configuration, and optical coupling properties. In this paper, an Au/Ag/SBA-15 nanocomposite was developed to study the plasmonic activities and optical properties. The potential improvement in optical properties as a result of changing the component ratios was investigated. Overall characterization of the samples was performed by X-ray diffraction analysis, transmission electron microscopy, Fourier transform infrared spectroscopy, nitrogen adsorption-desorption isotherm measurement, photoluminescence, and UV-Vis spectroscopy. Since tuning and improving the plasmonic properties and photoluminescence emission is challenging, this knowledge is valuable to predict the behavior of Au/Ag/SBA-15 nanocomposites to different combinations and synthetic methods.

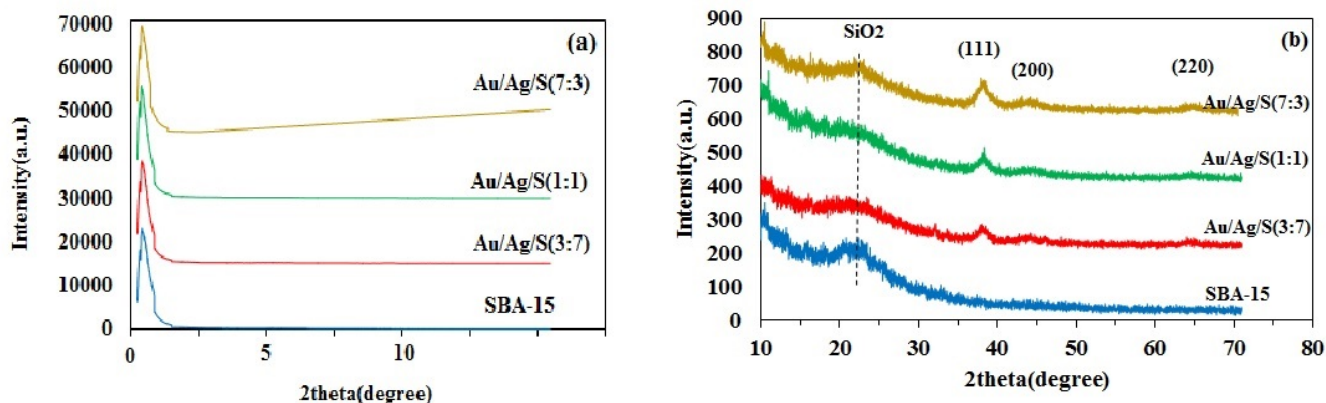


Figure 1. X-ray diffraction patterns of mesoporous silica SBA-15, Au/Ag/S (3:7), Au/Ag/S (1:1) and Au/Ag/S (7:3) nanocomposite at (a) low- angle (0-10 degrees) and (b) wide- angle (10-70 degrees).

2. Experimental procedure

2.1 Chemicals

Tri-block copolymer Pluronic (P123, EO20PO70 EO20), tetra ethyl orthoacetate (TEOS), and 3,3-aminopropyl trimethoxysilane (APTMS) were purchased from Sigma-Aldrich Company. Tetrachloroauric acid (HAuCl₄), silver nitrate (AgNO₃), ammonia solution, n-hexane, HCl and ethanol were purchased from Merck Company. All chemicals were of analytical grade and used as received.

2.2 Synthesis of mesoporous silica SBA-15

Mesoporous silica SBA-15 was synthesized according to the Zhao's method using P123 and TEOS as template and silica source, respectively [18]. First, P123 (4.0 g) was dissolved in the solution of water (30 cc) and HCl (2M, 120 g) while stirring at 35°C. After a uniform dispersion was obtained, 8.50 g of TEOS was added to the mixture with stirring for 24 hours. Then the mixture was aged at 80°C overnight. Thereafter, the product was filtered, washed and dried at room temperature. The calcination was performed while slowly raising the temperature from room temperature to 500°C in 8 hours and holding at 500°C for 6 hours. As known, the functionalization of mesoporous silica SBA-15 introduces a coordination and an end cap that facilitates the attachment of metal nanoparticles to the SBA-15 matrix [15–17]. For functionalization, APTMS solution (2 w%) was used as the amino acid agent. The solution of SBA-15 (1 g), ethanol and APTMS (50 cc) was stirred for 3 h to fix the APTMS attachment to the channel surfaces. Finally, the product was washed with ethanol and dried at 60°C.

2.3 Preparation of Au/Ag/SBA-15 nanocomposite

To prepare an Au/Ag/SBA-15 nanocomposite, 1 g of functionalized SBA-15 was added to the aqueous precursor solution of HAuCl₄ (1 mM) and AgNO₃ (1 mM). The solution remained on the stirrer for 3 h at room temperature until the solution changed color, confirming the formation of reduced metal NPs. Then it was filtered and washed with ammonia solution

and deionized water. The sample was air-dried at 60°C for one day and finally calcined at 300°C at a rate of 1°C/1 min. In this way, three samples with different weight ratios of HAuCl₄ (aq.) to AgNO₃ solutions (3:7, 1:1 and 7:3) were successfully prepared. The prepared nanocomposite powders were prepared according to the different weight ratios of HAuCl₄ (aq.) to AgNO₃ (aq.) solutions.

2.4 Characterization

The prepared samples were characterized by various structural and optical analyzes as follows. The Siemens D500 powder diffractometer was applied to obtain an XRD pattern of samples using CuK radiation (wavelength = 1.5418 nm). XRD analysis was recorded using 2 varying from 0.5 to 10 degrees for the small-angle case to identify the characteristic hexagonal lattice peak of SBA-15. Wide-angle (10 to 70 degrees) XRD analysis was used to identify any crystalline structure. The morphology of the samples was examined by transmission electron microscopy (Zeiss, EM10C, Germany) at 100 kV voltage. FTIR spectroscopy was established in the range of 400-4000 cm⁻¹ (Bruker Quinox 55). The surface area and pore size distribution of mesoporous structures were studied using the BET technique (HORIBA Scientific) and the nitrogen adsorption-desorption isotherm curve. The absorption spectra were measured with a Lambda 850 UV spectrometer and photoluminescence spectroscopy using a xenon arc lamp (excitation wavelength = 325 nm, 860 mW).

3. Results and discussion

Figure 1(a) shows the small-angle (0-10) X-ray diffraction pattern for all samples. The characteristic SBA-15 peak is clearly seen at an angle of about 1.7~2, which corresponds to the p6mm symmetry of the hexagonal lattice of the mesoporous silica SBA-15 for all samples [18]. The presence of this peak in the small-angle diffraction pattern of all nanocomposites clearly shows that the mesoporous structure is retained after metal loading. Very small changes in peak intensity are observed by changing the amount of charged nanoparticles

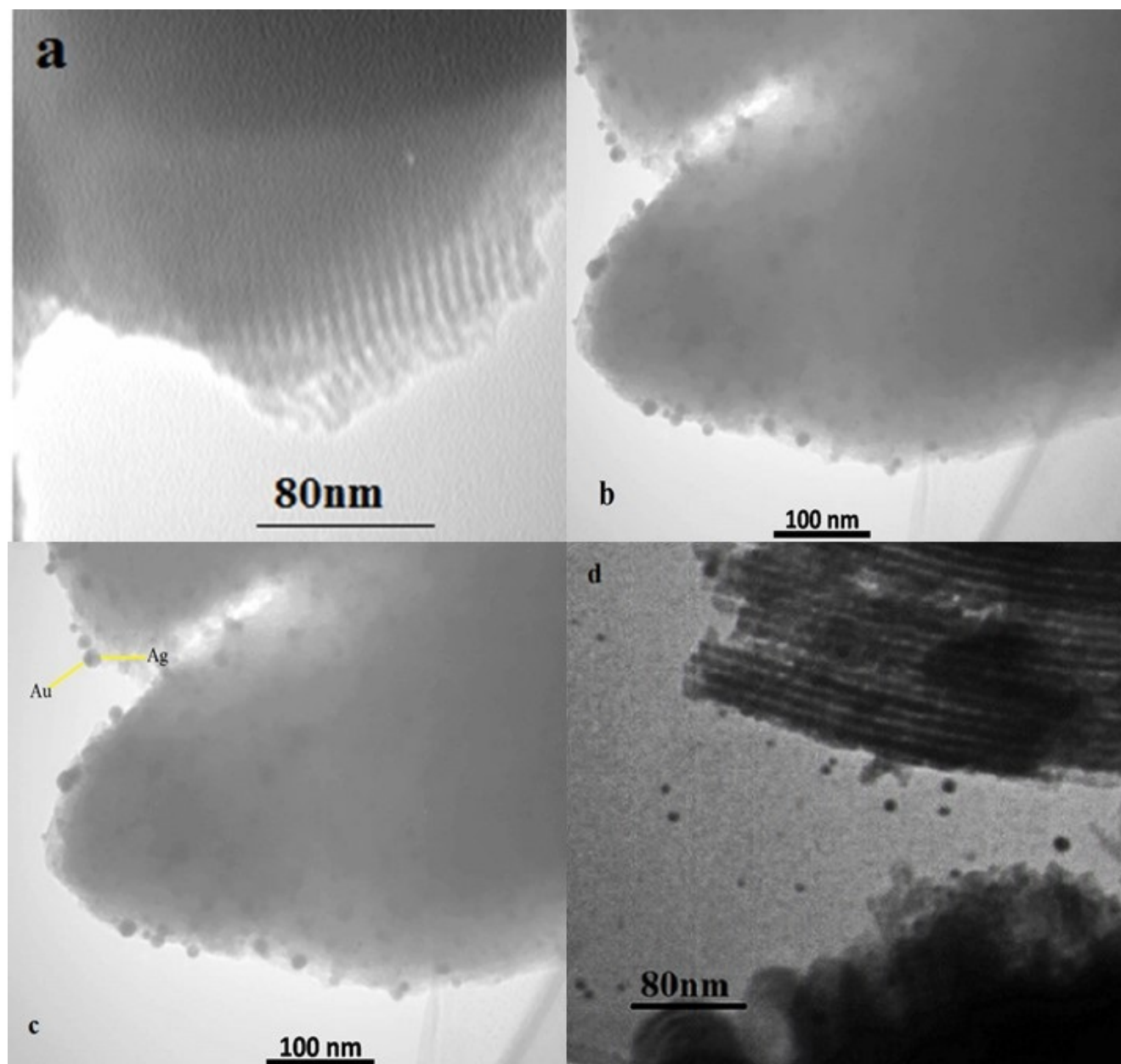


Figure 2. TEM images for (a) SBA-15 sample, (b) Au/Ag/S (3:7), (c) Au/Ag/S (1:1) and (d) Au/Ag/S (7:3) nanocomposites.

in different samples. This could be due to the pore filling of SBA-15 after the formation of metal nanoparticles and hence the changes in the lattice parameters of SBA-15. The wide-angle diffraction pattern of nanocomposites is shown in Figure 1(b). The broad peak of the amorphous structure of mesoporous SiO₂ silicon walls is observed for all samples. In general, SBA-15 does not have a specific peak in the range of $2\theta=10$ to 70 [6, 18]. The Au/Ag/S (1:1) nanocomposite shows three diffraction peaks at angles 2,38.32, 44.1 and 64.06, corresponding to the (111), (200) and (220) points, respectively. These peaks relate to the face centered cubic (FCC) gold lattice (JCPDS-04-0784 and JCPDS-87-0717). Since Au and Ag nanoparticles have the same lattice constants (0.408 and

0.409 nm), the XRD pattern of bimetallic Au-Ag nanoparticle is similar to that of monometallic Au nanoparticles [10–14]. As can be seen, other samples show similar diffraction peaks, the properties of which are listed in Table 1. The crystal size in Table 1 was estimated using the well-known Scherrer formula [19].

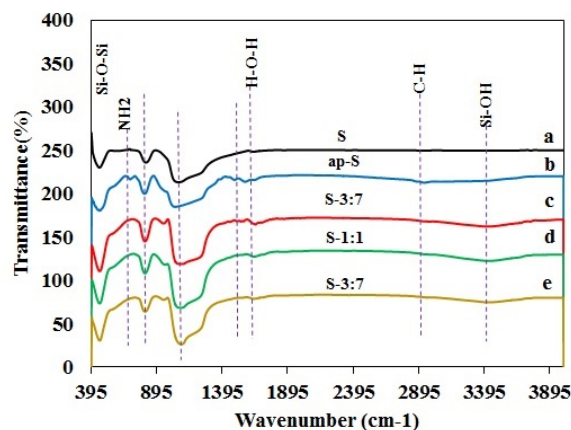
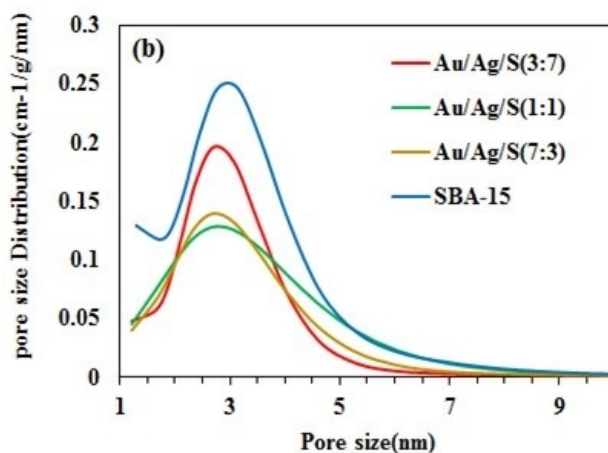
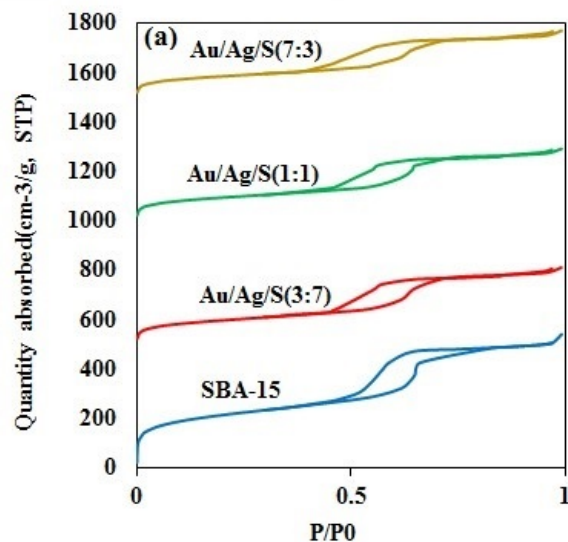
The TEM images of mesoporous silica SBA-15 and bimetallic nanocomposites are shown in Fig. 2 (a-d). The honeycomb morphology with parallel, straight channels and uniform pores for the bare matrix of SBA-15 is shown in Figure 2(a). It agrees with the low-angle XRD results. The pore diameter size was estimated to be 3 nm for SBA-15 according to the measurement software. Figures 2 (b-d) show the TEM im-

Table 1. Wide-angle (10-70 degree) XRD data of Au/Ag/S (3:7), Au/Ag/S (1:1) and Au/Ag/S (7:3) nanocomposites.

Nano composite	Peak Position($^{\circ}$)	hkl	Rel. Int (%)	Crystallite Size(nm)
Au/Ag/S(3:7)	38.08	(111)	39.01	15.5
	44.13	(200)	11.42	18.5
	64.29	(220)	10.48	15.1
Au/Ag/S(1:1)	38.32	(111)	0.24	18.1
	43.10	(200)	0.05	22.1
	64.06	(220)	0.03	12.3
Au/Ag/S(7:3)	38.11	(111)	19.43	7.70
	44.05	(200)	5.70	18.50
	64.61	(220)	3.05	5.50

ages of Au/Ag/S (3:7), Au/Ag/S (1:1), and Au/Ag/S (7:3) nanocomposites, respectively. Metal nanoparticles are observable in the channels and on the surface of the SBA-15 matrix. The difference in the contrast of the nanoparticle zones shows that Au-Ag nanoparticles were formed in a way that the darker zone is probably attributed to Au and the lighter zone corresponds to Ag nanoparticles [20,21]. In addition, it is evident that the bimetallic nanocomposites have the ordered two-dimensional hexagonal structure of mesoporous silica SBA-15.

Figure 3 shows the result of FTIR analysis for pristine SBA-15, functionalized SBA-15 and Au/Ag/S bimetallic nanocomposites. The adsorption bands at 464 cm^{-1} (Si-O-Si bending mode), 821 cm^{-1} (Si-O-Si stretching mode), 958 cm^{-1} (Si-OH-Si mode) and 1080 cm^{-1} (Si-O-Si symmetric stretching) are common in the typical FTIR analysis of SBA-15 [22,23]. The adsorption band at 3420 cm^{-1} is related to the OH groups

**Figure 3.** FTIR spectrum for (a) bare SBA-15 sample, (b) functionalized SBA-15 sample, (c) Au/Ag/S (3:7), (d) Au/Ag/S (1:1) and (e) Au/Ag/S (7:3) nanocomposites.**Figure 4.** Nitrogen adsorption-desorption isotherms (a) and pore size distribution curves (b) for mesoporous silica SBA-15, Au/Ag/S (3:7), Au/Ag/S (1:1) and Au/Ag/S (7:3) nanocomposites at standard temperature and pressure (STP).

of vibrational strain and the peak generated at 1650 cm^{-1} corresponds to the N-H vibrational band. The FTIR spectrum of the Au/Ag/S bimetallic nanocomposites shows that the peak intensity varies due to the changes in the electronic configuration of the bound groups.

BET analysis was performed to investigate the changes induced in the textural properties of the samples after loading with Au/Ag nanoparticles. Figure 4 shows (a) the N_2 adsorption-desorption isotherms and (b) the size distribution of the pores in the prepared samples. The hysteresis loop for all samples can be seen in Fig.4(a). A typical type IV isotherm is given, which is a typical feature of mesoporous-based nanocomposites. Furthermore, it confirms the preservation of the mesoporous structure and the existence of hexagonal cylindrical channels after loading with metal nanoparticles.

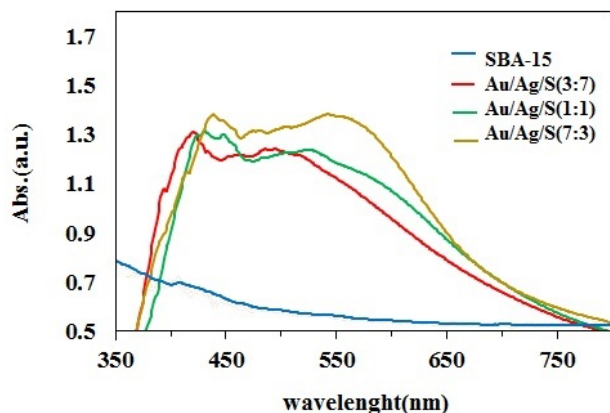


Figure 5. Absorption spectra of mesoporous silica SBA-15 and Au/Ag/S nanocomposites.

In the pore size distribution diagram, a significant change is observed after the incorporation of Au/Ag nanoparticles into the mesoporous silica SBA-15 (Fig. 4(b)). The texture parameters of the samples including specific surface area (SBET), total pore volume (V_{total}) and average pore diameter (r_p) were summarized in Table 2. As can be seen, after loading Au/Ag bimetallic nanoparticles, the specific surface area, total pore volume, and average pore diameter are significantly decreased due to the inclusion of Au-Ag nanoparticles in the pores of mesoporous silica SBA-15. It appears that the results from BET are consistent with the results from XRD and TEM analysis.

Figure 5 shows the UV-Vis absorption spectra of all samples. Two peaks are observed for all three bimetallic nanocomposite samples, indicating the plasmonic properties of the Au and Ag nanoparticles. For example, an Au/Ag/S (1:1) nanocomposite exhibits two major bands at 420 and 540 nm. As can be seen, the position of the peaks has changed by changing the ratio of the aqueous precursor solution of HAuCl₄ (1mM) and AgNO₃ (1mM). This could be due to the different configurations of conduction electrons at the surface and interface between Au and Ag nanoparticles. One of the main advantages of plasmonic Au and Ag bimetallic nanocomposites is their ability to engineer the collective conduction mode. In general, the properties of plasmonic modes strongly depend on the size, shape, and composition of the bimetallic nanocomposites. As

Table 2. Textural properties of mesoporous silica SBA-15, Au/Ag/S (3:7), Au/Ag/S (1:1) and Au/Ag/S (7:3) nanocomposites (extracted from BET measurements).

Sample	S_{BET} (m ² /g)	V_{total} (cm ³ /g)	r_p (nm)
SBA-15	755.74	137.63	3.2
Au/Ag/S(3:7)	346.27	79.55	2.7
Au/Ag/S(1:1)	334.33	76.81	2.7
Au/Ag/S(7:3)	301.79	69.33	2.7

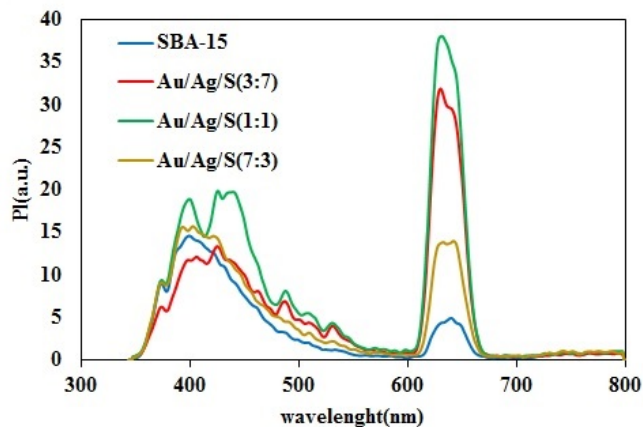


Figure 6. Photoluminescence spectra of mesoporous silica SBA-15 and Au/Ag/S nanocomposites under excitation at 325 nm at Room temperature.

As a result, the absorption bands of Au/Ag/S nanocomposites experience a red shift by increasing the gold concentration. Figure 6 shows the PL spectra of prepared samples under 325 nm irradiation at room temperature. Two emission peaks centered at 410 and 640 nm are observed in the spectrum of SBA-15 mesoporous silica. The emission at 410 nm could be related to the edge of the SiO₂ bond, the surface states of the Si-OH bond and the hydroxyl groups, while the other peak is mainly due to the defects in oxygen sites and surface states [6, 24]. The emission spectra of bimetallic nanocomposites show no significant change in position or peak numbers. However, in the wavelength range of 640 nm, a clear increase in peak intensity is observed, especially for Au/Ag/S (1:1) nanocomposite. The increase in peak intensity of Au/Ag/S nanocomposites is mainly related to the new electronic configurations, formation of surface/interface states, and efficient charge transfer. Most of the active emission sites of gold and silver nanoparticles have been attributed to the radiative recombination of an electron-hole pair between the d-band and the sp-band [16]. Due to plasmon resonance excitation, it is found that the local field generated around the plasmonic metal nanoparticles modifies the electronic configurations and active sites. Furthermore, the electronegativity of Au nanoparticles is larger than that of Ag nanoparticles, resulting in the formation of a strong electronic bond that causes efficient charge transfer from gold to silver [10]. It appears that more active surface/interface sites have been created in the Au/Ag/S (1:1) nanocomposite, where the probability of 640 nm transitions is increased. By further increasing the amount of Au, the peak intensity at 640 nm underwent a remarkable decrease in the Au/Ag/S (7:3) nanocomposite. Probably due to the saturation of the two metals, the mesoporous become partially blocked and the surface/interface fluorescently active sites are reduced.

4. Conclusion

In this work, the functionalized mesoporous silica SBA-15 was successfully modified by plasmonic Au/Ag bimetallic nanoparticles to enhance the photoluminescence emission in the red wavelength range. XRD, TEM, FTIR, and BET experiments were performed to investigate structural and physicochemical properties. According to the results, the uniform pores and regular honeycomb structure of the mesoporous SBA-15 were observed before and after loading Au/Ag bimetallic nanoparticles. TEM images show that bimetallic Au/Ag nanoparticles were deposited in the channels and on the surface of the SBA-15 matrix. It correlated well with the decreases in BET specific surface area, total pore volume, and average pore diameter after loading Au/Ag bimetallic nanoparticles. The optical properties of Au/Ag/S nanocomposites were studied by UV/Vis and photoluminescence spectroscopy. UV/Vis spectroscopy showed the plasmonic bands of Au as well as those of Ag nanoparticles. In addition, a red shift was seen in the absorption bands of Au/Ag/S nanocomposites as the gold concentration was increased. In the photoluminescence spectrum of the Au/Ag/S (1:1) nanocomposite, an enhanced emission at 640 nm was observed due to the formation of more active sites and efficient charge transfer. The enhanced emissions from Au/Ag/S nanocomposites in the red wavelength range can be used to identify biological molecules. However, further investigations are needed for desirable applications.

Conflict of interest statement:

The authors declare that they have no conflict of interest.

References

- [1] R. Liu, Y. Shi, Y. Wan, Y. Meng, F. Zhang, D. Gu, Z. Chen, B. Tu, and D. Zhao. *Journal of the American Chemical Society*, **128**:11652, 2006.
- [2] P. Van Der Voort, P. Ravikovitch, K. De Jong, M. Benjelloun, E. Van Bavel, A. Janssen, A. Neimark, B. Weckhuysen, and E. Vansant. *Journal of Physical Chemistry B*, **106**:5873, 2002.
- [3] J. M. Rosenholm, C. Sahlgren, and M. Linden. *Nanoscale*, **2**:1870, 2010.
- [4] B. Sahoo, K. S. P. Devi, S. Dutta, T. K. Maiti, P. Pramanik, and D. Dhara. *Journal of Colloid and Interface Science*, **431**:31, 2014.
- [5] R. Sharma, S. Sharma, S. Dutta, R. Zboril, and M. B. Gawande. *Green Chemistry*, **17**:3207, 2015.
- [6] S. Estakhri, E. Darabi, B. Akbari-Adergani, and S. M. Elahi. *Journal of Porous Materials*, **28**:989, 2021.
- [7] Y. Min and Y. Wang. *Frontiers in Chemistry*, **8**:411, 2020.
- [8] K. Sytwu, M. Vadai, and J. A. Dionne. *Advances in physics:X*, **4**:1619480, 2019.
- [9] P. Verma, Y. Kuwahara, K. Mori, R. Raja, and H. Yamashita. *Energy Chem.*, **4**:100070, 2022.
- [10] K. Loza, M. Heggen, and M. Epple. *Advanced Functional Materials*, **30**:1909260, 2020.
- [11] M. Chen, Y. He, and J. Zhu. *International Journal of Heat and Mass Transfer*, **114**:1098, 2017.
- [12] J. Zhu, X. Li, J. Li, and Jun wu Zhao. *Spectrochimica Acta Part A: Molecular and Biomolecular Spectroscopy*, **189**:571, 2018.
- [13] A. V. Korotun and V. Pogosov. *Physics of the Solid State*, **63**:122, 2021.
- [14] A. Scala, G. Nerj, N. Micale, M. Cordaro, and A. Piperno. *Molecules*, **27**:1134, 2022.
- [15] P. verma, Y. Kuwahara, K. Mori, and H. Yamashita. *Journal of Materials Chemistry A*, **4**:10142, 2016.
- [16] P. Verma, K. Yuan, Y. Kuwahara, K. Mori, and H. Yamashita. *Applied Catalysis B: Environmental*, **223**:10, 2018.
- [17] E. Chiani, S. N. Azizi, and Sh. Ghasemi. *International Journal of Hydrogen Energy*, **46**:25468, 2021.
- [18] D. Zhao, Q. Huo, J. Feng, B. F. Chmelka, and G. D. Stucky. *American Chemical Society*, **120**:6024, 1998.
- [19] B. D. Cullity and S. R. Stock. *Elements of x-ray diffraction*. Prentice Hall. Upper Saddle River, NJ, 11th edition, 2001.
- [20] L. Yang, M. Qi, and M. Jin. *Cryst. Eng. Comm.*, **15**:2804, 2013.
- [21] N. Berahim, W. J. Leo, B. F. leo, and M. R. Johan. *Catalysts*, **8**:412, 2018.
- [22] B. Valeur and I. Leray. *Coordination chemistry Reviews*, **3**:205, 2000.
- [23] J. Notorio, E. H. M. Nunes, D. C. L. Vasconcelos, and W. L. Vasconcelos. *Journal of Porous Materials*, **26**:1581, 2019.
- [24] L. Gai, H. Jiang, D. Cui, and Q. Wang 120 (2009) 410. *Microporous and Mesoporous Materials*, **120**:410, 2009.